THE 8th STUDENT SYMPOSIUM ON MECHANICAL AND MANUFACTURING ENGINEERING

Design of motion controller for permanent magnet synchronous motor

Mathias G. Pedersen, Patrick W. Nielsen, Lars Peter B. Rask, Eiden A. Harmen, Gustas Kaminskas

Department of Materials and Production, Aalborg University
Fibigerstraede 16, DK-9220 Aalborg East, Denmark
E-mail: {mgpe17, pwni15, lrask15, earred20, gkamin20}@student.aau.dk
Web page: http://www.mechman.mp.aau.dk/

Abstract

This project concerns the development of cascade speed- and current control of a magnetically geared permanent magnet synchronous motor (PMSM) winch drive, to be used for an industrial hoisting system. The dynamic model of the winch drive is developed as both a rigid system and another including the torsional spring effect of the magnetic gear. A cascade controller was designed for the linearized rigid system and tested in simulations on both the rigid and torsional spring system. It was found that the designed controller could sufficiently control the spring system on speed ramps and load steps, eliminating the steady state error and ensuring negligible overshoot.

Keywords: Winch drive, PMSM, coaxial magnetic gear, field oriented control

Nomenclature

The subscript k in the following list indicates the phases A, B, and C.

u_{k}	Voltage $[V]$
i_{k}	Current $[A]$
R_{s}	Coil resistance $[\Omega]$
L_{k}	Inductance $[H]$
ϵ_{k}	Back- emf voltage $[V]$
L_{m}	Mutual inductance $[H]$
ψ_{k}	Magnetic flux linkage $[Wb]$
$\psi_{\mathrm{pm(k)}}$	Magnetic flux from the permanent magnets $[Wb]$
$\psi_{\mathrm{L(k)}}$	Magnetic flux contribution form phase k to the remaining phases $[Wb]$
ϵ_{km}	Flux contribution of surrounding phases to phase k $[V]$
ϵ_{kpm}	Back-emf contribution of permanent magnets to phase k $[V]$
λ_{pm}	Amplitude of permanent magnet flux linkage $[Vs/Hz]$
θ_{e}	Electrical angle $[rad]$
P_{k}	Power $[W]$
P_{in}	Input power to the motor $[W]$
G	Magnetic gear gearing ration [-]
G_{p}	Pulley gearing [-]
pp_{HSR}	Number of HSR pole pairs [-]
pp_{LSR}	Number of LSR pole pairs [-]
p	Number of poles [-]
θ_{HSR}	Angular position of HSR $[rad]$
θ_{LSR}	Angular position of LSR $[rad]$
J_{HSR}	HSR mass moment of inertia $[kg\ m^2]$
J_{LSR}	LSR mass moment of inertia $[kg\ m^2]$
B_{HSR}	HSR viscous damping coefficient $[Nms]$
B_{LSR}	LSR viscous damping coefficient $[Nms]$
τ_e	Electrical torque of the motor $[Nm]$
τ_L	Torque produced by the load $[Nm]$

1. Introduction

The aim of this paper is to investigate the effect of the torsional spring effect that exists in a coaxial magnetic gear, in comparison to the same coaxial gear considered as a rigid system. The high-speed rotor (HSR) of the magnetic gear is the driving shaft, and is powered by a permanent magnet synchronous motor (PMSM). The low-speed rotor side of the gear (LSR) is the output shaft, and is joined with a winch drum, allowing the spooling of wire as part of a hoisting system. The wire is further put through a pulley at the hook of the hoisting system, providing another gearing ratio of two. The goal of using the PMSM and magnetic gear drive combination is to gain knowledge of how the motion of the system is affected when the torsional spring effect of the gear is included.

Due to the physical system not being assembled at the time of writing this paper, no experiments on the physical system have been performed. Instead, the non-linear simulation model serves as the subject for the controller implementation and experiment setup.

2. Electrical model of the PMSM

The three phases of the permanent magnet synchronous motor are connected in a star configuration as can be seen on the figure below:

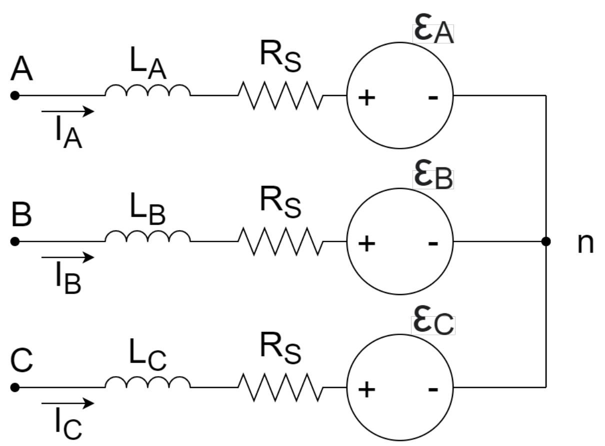

Fig. 1 A figure showing the star connection configuration of the PMSM.

Seen on the figure are L_A, L_B and L_C which are the phase inductances, R_S which is the phase resistance, ϵ_A, ϵ_B and ϵ_C which are the phase back electromotive forces and I_A, I_B and I_C which are the phase currents. For this paper, the phase inductances and resistances are assumed to be equal. With Kirchhoff's voltage law [2], the voltage in each phase can be expressed as:

$$u_k = L_k \frac{di_k}{dt} + R_s i_k + \epsilon_k \tag{1}$$

Using Faraday's law [3], the back electromotive forces can be expressed as a change of magnetic flux crossing the conductor. Since this is a three-phase PMSM, the electromotive force depends on the flux contribution from the surrounding phases [1]:

$$\epsilon_A = \frac{d\psi_A}{dt} = \frac{d}{dt}(\psi_{L_B} + \psi_{L_C} + \psi_{pm_A}) \tag{2}$$

The electromotive force can be separated into the flux contribution of the surrounding phases and the flux contribution form the permanent magnets [1]:

$$\epsilon_k = e_{km} + e_{kpm} \tag{3}$$

Where ϵ_k is the flux contribution from the surrounding phases, which for phase A would be:

$$e_{Am} = L_m \left(\frac{di_B}{dt} + \frac{di_C}{dt} \right) \tag{4}$$

Where L_m is the mutual inductance. Using Kirchhoff's law again, this can be rewritten as:

$$e_{Am} = -L_m \frac{di_A}{dt} \tag{5}$$

The flux contributions from the permanent magnets from Equation 3 can be described as [1]:

$$\frac{d\psi_{pm_A}}{dt} = \lambda_{pm} \frac{d\gamma_A}{dt} \tag{6}$$

Where λ_{pm} is the amplitude of the flux linkage [4], and γ_k is the factor dependent on the phase and the angle of the electrical rotation θ_e, which can be expressed for each of the phases as [1]:

$$\gamma_A = \cos(\theta_e) \tag{7}$$

$$\gamma_B = \cos\left(\theta_e - \frac{2\pi}{3}\right) \tag{8}$$

$$\gamma_C = \cos\left(\theta_e - \frac{4\pi}{3}\right) \tag{9}$$

Inserting Equation 5 and 6 into Equation 1, and rearranging by combining inductances, the final voltage equation is obtained:

$$u_k = (L_k - L_m)\frac{di}{dt} + R_s i_k + \lambda_{pm}\frac{d\gamma_k}{dt} \quad \text{with } k \in \{A, B, C\} \tag{10}$$

2.1 Electromechanical torque

The next step is to relate the current i and the electrical torque τ_e, which is done here using the input power of the system which can be determined as [1]:

$$P_{in} = P_A + P_B + P_C \tag{11}$$

$$P_{in} = u_A i_A + u_B i_B + u_C i_C \tag{12}$$

This equation uses information from the three phases in order to calculate the power. Using the Clark and Park transformations, it is possible transform from the three phases A, B and C into the d, q coordinate system for both the voltage Equation 10 and the power Equation 12 [1]:

Voltage equation in d, q:

$$u_d = R_s i_d + L\frac{di_d}{dt} - \dot{\theta}_e L i_q \tag{13}$$

$$u_q = R_s i_q + L\frac{di_q}{dt} + \dot{\theta}_e (L i_d + \lambda_{pm}) \tag{14}$$

Power equation in d, q:

$$P_{in} = \frac{3}{2}(u_d i_d + u_q i_q) \tag{15}$$

Substituting the voltage equations into the power equation and rearranging, it is possible to obtain the following equation:

$$P_{em} = \tau_e \dot{\theta}_m = \frac{3}{2}(\dot{\theta}_e \lambda_{pm} i_q) \tag{16}$$

In order to obtain an equation for the electrical torque τ_e, the electrical angular velocity is transformed into mechanical angular velocity using the number of poles in the motor as seen below:

$$\dot{\theta}_e = \dot{\theta}_m \frac{p}{2} \tag{17}$$

and thereby yielding:

$$\tau_e = \frac{3p}{4}\lambda_{pm} i_q \tag{18}$$

The current equations i_d and i_q can be found from the voltage Equation 13 and 14 as can be seen below:

i_d:

$$\frac{di_d}{dt} = \frac{u_d - R_s i_d + \dot{\theta}_e L i_q}{L} \tag{19}$$

i_q:

$$\frac{di_q}{dt} = \frac{u_q - R_s i_q + \dot{\theta}_e L i_d - \dot{\theta}_e \lambda_{pm}}{L} \tag{20}$$

With these three final non-linear equations 18, 19 and 20, it is possible to build the non-linear electrical model of the PMSM motor.

2.2 Linearisation and Laplace of the PMSM electrical model

To build the linear model of the PMSM motor, these equations have to be linearised and Laplace transformed. To do this, for the current equations, the cross-coupling from i_q in Equation 19, and from i_d in Equation 20 is neglected. This is because it is assumed that the cross-coupling effect is negligible, and the controller is to be designed such that the current i_d is zero to maximize the torque. The electrical torque however, is already a linear expression. With this in mind, the linearisation and Laplace is performed and the following transfer functions are obtained:

τ_e:

$$\frac{\tau_e}{i_q} = \frac{3p}{4}\lambda_{pm} \tag{21}$$

i_d:

$$\frac{i_d(s)}{u_d(s)} = \frac{1}{sL + R_s} \tag{22}$$

i_q:

$$\frac{i_q(s)}{u_q(s)} = \frac{1}{sL + R_s} - \frac{\dot{\theta}_m(s)}{u_q(s)}\frac{p\lambda_{pm}}{2(sL + R_s)} \tag{23}$$

3. Rigid mechanical model

In order to derive the equations of motion for the mechanical model of the winch drive, a figure is made which shows how the system is to be modelled:

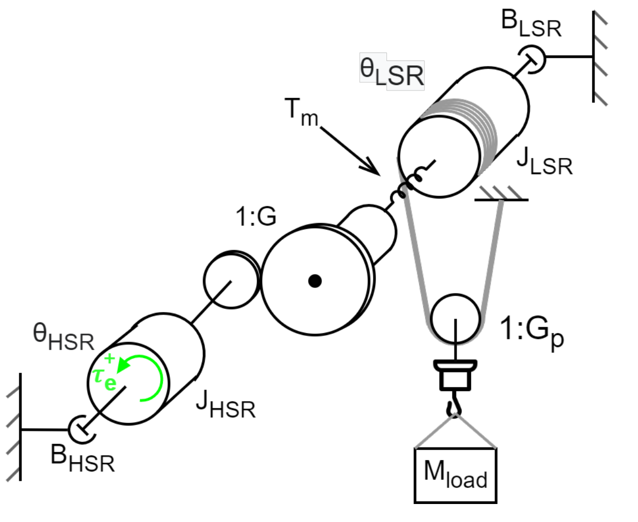

Fig. 2 A figure showing the magnetic gear winch drive configuration from which equations of motion is derived

The two cylindrical bodies J_{HSR} and J_{LSR} is the HSR and the LSR parts of the magnetic gear respectively.

There is a gearing of $1 : G$ between the two bodies and a torsional spring between the gear and the LSR. The mechanical system of the winch drive is in this section considered as a rigid system, where the torsional spring is assumed to be infinitely stiff. A pulley gear with ratio $1 : G_p$ is also added between the LSR and the load where the cable is also assumed infinitely stiff. An equation of motion is made for this one degree of freedom system with newtons second law:

$$\left(J_{\text{HSR}} + \frac{J_{\text{LSR}}}{G^2}\right)\ddot{\theta}_{\text{HSR}} = \tau_e - \left(B_{\text{HSR}} + \frac{B_{\text{LSR}}}{G^2}\right)\dot{\theta}_{\text{HSR}} - \tau_L \quad (24)$$

With the load torque referred to the HSR, stated as the static and dynamic loads, with the latter resulting from the HSR angular acceleration:

$$\tau_L = \frac{Mgr}{G_p G} + \frac{Mr^2}{G_p^2 G^2}\ddot{\theta}_{\text{HSR}} \quad (25)$$

Collecting the equivalent loading from the HSR acceleration to the left-hand side, the equivalent system mass moment of inertia is expressed:

$$\left(J_{\text{HSR}} + \frac{J_{\text{LSR}} + J_{WD}(\theta_{\text{LSR}})}{G^2} + \frac{Mr(\theta_{\text{LSR}})^2}{G_p^2 G^2}\right)\ddot{\theta}_{\text{HSR}} = \tau_e - \left(B_{\text{HSR}} + \frac{B_{\text{LSR}}}{G^2}\right)\dot{\theta}_{\text{HSR}} - \frac{Mgr(\theta_{\text{LSR}})}{G_p G} \quad (26)$$

3.1 Transfer function

In order to linearise Equation 26, the load is considered a disturbance and therefore is not included in the transfer function. Doing this, it is possible to Laplace transform the equation that results in the transfer function below:

$$\frac{\theta_{\text{HSR}}(s)\cdot s}{\tau_e} = \frac{1}{sJ_R + B_R} \quad (27)$$

The inertia contribution J_{WD} from the wire being wound onto the LSR drum is modelled as a linear expression depending on the angular position θ_{LSR}. The largest error between the linear expression and the nonlinear was less than 2%. Since the effective drum radius $r_{\theta_{\text{LSR}}}$ is included in the static load, its effects on the load torque applied on the LSR are considered part of the disturbance. An equivalent system inertia J_R is found by adding up the inertia terms on the left hand side of Equation 26. The same is done for the equivalent viscous damping coefficient B_R for which the HSR and LSR dampings have been combined.

4. Spring system mechanical model

The mechanical system including the torsional spring effect of the magnetic gear is considered as a system of two degrees of freedom, one for the HSR assembly and one for the LSR/drum assembly. The torsional spring between the gearing and the LSR is now included to describe the investigate the behaviour. The wire for this system is still considered rigid. The mathematical model of the mechanical system then consists of two simultaneous equations of motion, one for each of the aforementioned assemblies:

$$J_{\text{HSR}}\ddot{\theta}_{\text{HSR}} = \tau_e - T_t(\phi) - B_{\text{HSR}}\dot{\theta}_{\text{HSR}} \quad (28)$$

$$J_{\text{LSR}}\ddot{\theta}_{\text{LSR}} = T_t(\phi)G - B_{\text{LSR}}\dot{\theta}_{\text{LSR}} + \tau_L \quad (29)$$

Where $T_t(\phi)$ is the torque transfer expression of the magnetic gear [6], defined as:

$$T_t(\phi) = T_m \sin(\phi) \quad (30)$$

where:

$$\phi = p_{\text{HSR}}\theta_{\text{HSR}} + p_{\text{LSR}}\theta_{\text{LSR}} \quad (31)$$

4.1 Transfer function

To obtain a transfer function, the nonlinear equations are to be Laplace-transformed, but this requires a linearization of the non-linear terms. The only non-linear term from Equation 28 and 29 is the torque transfer expression given in Equation 30. It is linearized by a first order Taylor expansion around selected linearization points:

$$T_t(\phi) \approx T_t(\phi_0) + (\phi - \phi_0)\left[\frac{\partial}{\partial\phi}T_t(\phi)\right]_{(\phi_0,\theta_{\text{HSR0}},\theta_{\text{LSR0}})} \quad (32)$$

Which when evaluated becomes:

$$T_t(\phi) \approx T_m sin(\phi_0) + (\phi - \phi_0)\ T_m\cos(\phi_0) \quad (33)$$

To obtain a spring stiffness which is able to represent a realistic range of angular displacements between the HSR and LSR, the linearization points of θ_{HSR0} and θ_{LSR0} are both chosen to be 0. The torque transferred from a given angular displacement in either direction from this equilibrium point on the sine curve will be the same. Using the two chosen linearisation points allows for calculation of ϕ_0:

$$\phi_0 = p_{HSR}\theta_{HSR0} + p_{LSR}\theta_{LSR0} = 0 \tag{34}$$

Inserting the calculated ϕ_0 value of 0 and the slip torque T_m referred to the HSR side into Equation 33 now yields the linear torsion spring term:

$$T_t(\phi) \approx T_m\sin(\phi_0) + (\phi - \phi_0)T_m\cos(\phi_0) = k_m\phi \tag{35}$$

Inserting the linearized spring constant k_m into the non-linear equations, they can be Laplace transformed and expressed as the matrix-vector system in Equation 36:

$$\begin{bmatrix} K_1 & K_2 \\ K_3 & K_4 \end{bmatrix} \begin{Bmatrix} \theta_{\text{HSR}} \\ \theta_{\text{LSR}} \end{Bmatrix} = \begin{Bmatrix} \tau_e \\ 0 \end{Bmatrix} \tag{36}$$

where:

$$\begin{aligned} K_1 &= J_{\text{HSR}}s^2 + B_{\text{HSR}}s + k_m p_{\text{HSR}} \\ K_2 &= k_m p_{\text{LSR}} \\ K_3 &= -k_m p_{\text{HSR}}G \\ K_4 &= J_{\text{LSR}}s^2 + B_{\text{LSR}}s - k_m p_{\text{LSR}}G \end{aligned} \tag{37}$$

The system of two equations can be solved for θ_{LSR} by Cramer's rule. Dividing both sides by the electrical torque τ_e and multiplying both sides by s then yields the transfer function describing the angular velocity of the LSR with the electrical torque as input:

$$\frac{s\theta_{\text{LSR}}}{\tau_e} = \frac{k_m p_{\text{HSR}}G}{D_1s^3 + D_2s^2 + D_3s + D_4} \tag{38}$$

where:

$$\begin{aligned} D_1 &= J_{\text{HSR}}J_{\text{LSR}} \\ D_2 &= B_{\text{HSR}}J_{\text{LSR}} + B_{\text{LSR}}J_{\text{HSR}} \\ D_3 &= -GJ_{\text{HSR}}k_m p_{\text{LSR}} + J_{\text{LSR}}k_m p_{\text{HSR}} + B_{\text{HSR}}B_{\text{LSR}} \\ D_4 &= -B_{\text{HSR}}Gk_m p_{\text{LSR}} + B_{\text{LSR}}k_m p_{\text{HSR}} \end{aligned} \tag{39}$$

Note that the configuration of the magnetic gear modulator the gearing ratio G is negative, ensuring a positive characteristic equation.

5. Controller design

With the transfer functions for the linear systems found, it is now possible to begin designing the PI controller for the rigid system to then apply it on the spring system. For an easier read, the main equations are rewritten here. The current equations are obtained from Equation 13 and 14. The electrical torque is found in subsection 2.1 and the rigid and spring system equations can be found in subsection 3.1 and 4.1 respectively.

i_d:

$$\frac{i_d(s)}{u_d(s)} = \frac{1}{sL + R_s} \tag{40}$$

i_q:

$$\frac{i_q(s)}{u_q(s)} = \frac{1}{sL + R_s} - \frac{\dot{\theta}_m(s)}{u_q(s)}\frac{p\lambda_{pm}}{2(sL + R_s)} \tag{41}$$

τ_e:

$$\frac{\tau_e}{i_q} = \frac{3p}{4}\lambda_{pm} \tag{18}$$

Rigid system:

$$\frac{\theta_{\text{HSR}}(s) \cdot s}{\tau_e} = \frac{1}{sJ_R + B_R} \tag{27}$$

These transfer functions can be represented in a block diagram as can be seen below:

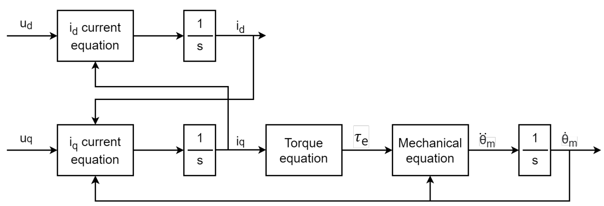

Fig. 3 Block diagram showing how the nonlinear rigid system simulation model is built.

Because these equations have been linearised and Laplace transformed, some linear control theory can be applied. In this case, pole-zero cancellation is applied.

5.1 Current controller

The first of the two controllers desgined is the inner loop controller for the current. The transfer function for this loop is shown below:

$$\frac{i_q}{i_{ref}} = \left(K_{pc} + \frac{K_{ic}}{s}\right)\left(\frac{1}{sL + R_s}\right) \tag{42}$$

The aim is to place the zero of the PI controller such that the plant transfer function pole is cancelled. The response of the system, then depends entirely on the designed PI controller. To do this, some rearranging of Equation 42 is necessary where, on the first parenthesis, s has been used as a common denominator and K_{ic} has been multiplied and divided by K_{pc} so it can be taken out as a common factor. In the second parenthesis, L has been divided on all terms to obtain a standard first order transfer function [5]:

$$\frac{i_q}{i_{ref}} = K_{pc}\left(\frac{s + \dfrac{K_{ic}}{K_{pc}}}{s}\right)\left(\frac{\dfrac{1}{L}}{s + \dfrac{R_s}{L}}\right) \tag{43}$$

Because it is assumed that R_s and L are constant, Equation 44 the following condition is made [5]:

$$\frac{K_{ic}}{K_{pc}} = \frac{R_s}{L} \tag{44}$$

With Equation 44, the pole and zero are cancelled out and therefore Equation 43 can be simplified to Equation 45:

$$\frac{i_q}{i_{ref}} = \frac{1}{\left(\dfrac{L}{K_{pc}}\right)s} \tag{45}$$

From [5] the relation between Equation 45 and the bandwidth for the controller is found and the equation is as follows:

$$|G_c(j\omega_{cc})| = \frac{1}{\left|\dfrac{L}{K_{pc}} j\omega_{cc}\right|} = 1 \rightarrow \omega_{cc} = \frac{K_{pc}}{L} \tag{46}$$

From Equation 46, the proportional gain for the controller can be found, and with it, the integral gain can be found using Equation 44.

$$K_{pc} = L\omega_{cc} \tag{47}$$

$$K_{ic} = R_s\omega_{cc} \tag{48}$$

To apply the speed controller on cascade form, this open loop controller has to be closed. Once this is done, the closed loop transfer function is as follows [5]:

$$\frac{i_q}{i_{ref}} = \frac{\omega_{cc}}{s + \omega_{cc}} \tag{49}$$

5.2 Speed controller

The speed controller is applied in cascade with the current controller. This one is the outer loop of the system and is the one controlling the speed. The transfer function for the open loop system is shown below:

$$\frac{\dot{\theta}_m}{\dot{\theta}_{m,ref}} = \left(K_{ps} + \frac{K_{is}}{s}\right)\left(\frac{\omega_{cc}}{s + \omega_{cc}}\right) \cdot \left(\frac{3p\lambda_{pm}}{4}\right) \cdot \left(\frac{1}{sJ_R + B_R}\right) \tag{50}$$

The bandwidth for the speed controller ω_{cs} is chosen to be ten times smaller than that of the current controller ω_{cc} in order for it not to be affected by the current control loop [5]. With this in mind, the current controller gain becomes approximately one when near the speed controller bandwidth ω_{cs} and therefore, current controller is assumed to not affect the speed controller [5].

$$G_c(s) = \frac{\omega_{cc}}{s + \omega_{cc}} \approx 1 \tag{51}$$

If the cutoff frequecy ω_{pi} of the speed PI controller is much smaller than the bandwidth ω_{cs} of the speed controller [5], then the PI speed controller transfer function can be reduced:

$$G_{pi}(s) = K_{ps} + \frac{K_{is}}{s} \approx K_{ps} \tag{52}$$

With these approximations for the controllers, Equation 50 can be reduced to:

$$\frac{\dot{\theta}_m}{\dot{\theta}_{m,ref}} = (K_{ps})\left(\frac{3p\lambda_{pm}}{4}\right)\left(\frac{1}{sJ_R + B_R}\right) \tag{53}$$

From [5], the open loop transfer function gain at frequency ω_{cs} is 0 dB as seen below:

$$|G_s(j\omega_{cs})| = 0 \text{ dB} \tag{54}$$

From this, the proportional gain K_{ps} and integral gain K_{is} for the speed controller can be found [5]:

$$K_{ps} = \frac{4(J_R \cdot \omega_{cs} + B_R)}{3p\lambda_{pm}} \tag{55}$$

$$K_{is} = \frac{K_{ps}\omega_{cs}}{5} \tag{56}$$

6. Comparison

To compare how the designed controller in the previous section performs on the two different systems, some experiments are made on their respective simulation models. These simulations show ramp inputs that accelerate and decelerate the system with an absolute value of 35 rad/s^2. The first comparison is of the angular velocity of the rigid and spring systems:

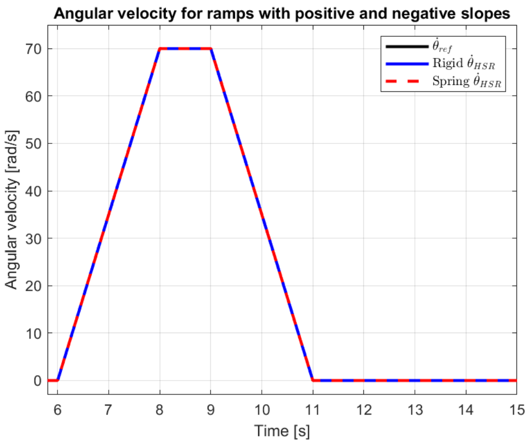

Fig. 4 Angular velocity response for the models when a ramp input with positive and negative slopes is applied

Figure 4, shows that the angular velocity response of the models follows the described input and a difference between the models is not observed. The next figure to be studied is the response of electrical torque with the same input as for Figure 4:

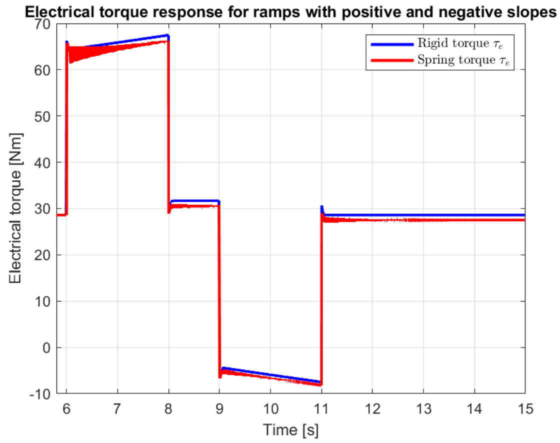

Fig. 5 Angular velocity response for the models when a ramp input with positive and negative slopes is applied

As can be seen from Figure 5, the electrical response from the electrical torque is different for the rigid and spring models. Oscillations from the spring model can be observed and related to the torsional spring effect of the magnetic gear. These oscillations are greater when the acceleration of the HSR is changing.

So far, the models have been compared such that the spring in the gear has been excited by the acceleration of the motor. By applying a disturbance while the angular velocity is constant, it is also possible to energize the spring and, therefore, possibly observe different behaviours in the systems.

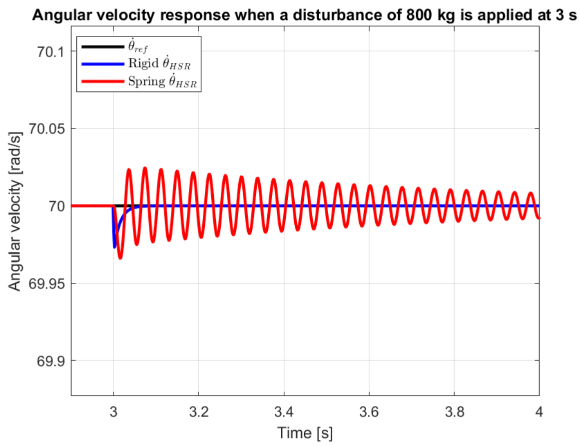

Fig. 6 Angular velocity response when a disturbance of 800 kg is applied at 3s

Figure 6 shows that for both the rigid and spring system, the controller is capable of compensating for the disturbance. In the rigid model the controller is able to counteract this load disturbance of 800 kg in under 0.1s with the angular velocity changing less than 0.05 rad/s. The controller in the spring system tries to compensate for the change in angular velocity but starts oscillating with an amplitude of less than 0.05 rad/s that slowly decreases. The reason behind this is that the controller does not take into account the torsional spring effect and for that reason oscillates.

In conclusion, in order to obtain the same results in the simulations, the torsional spring effect would have to be taken into account when designing a controller. One way of achieving this could be to implement a feedforward compensator that would compensate for the load disturbance. In this case, a good evaluation of the load and its transfer function would be necessary.

7. Discussion

In both models of the PMSM winch drive, an additional complexity to study would be the inclusion of the wire stiffness. The wire stiffness would be a new non-linearity, as the stiffness of the wire would depend on the length. This would require a linearisation around a desired lifting point along the height of the wind turbine, from where a constant stiffness would be found. This additional degree of freedom of the load mass would open up investigation of additional oscillations caused by this phenomenon.

More investigation would also have to be made about the applied load step at a fixed angular velocity of the HSR in Figure 6. The mass of 800 kg caused a speed decrease of only of 0.025 rad/s on the reference speed of 70 rad/s on the HSR, and recovered in approximately 0.07 s. However this quick correction could be caused by the equivalent HSR mass moment of inertia of over 600 kgm^2 when referred to the LSR-side on the other side of the magnetic gear.

8. Conclusion

From the comparisons in section 6, it can be concluded that the cascade controller designed for the rigid system was able to sufficiently control the spring system, as it showed similar results for both systems. Highlights from these were the controller's ability to keep the load steady at zero velocity, and maintain a steady state error of negligible magnitude ($< 1\%$), also when lifting and descending the load. The current controller was able to stay within the maximum torque rating of the motor when given load steps and ramp inputs on the speed.

The controller had difficulty reducing oscillations when a load step was applied while running at a fixed speed, however the amplitude of these oscillations was of negligible magnitude, in that the speed oscillated with an amplitude of approximately 0.025 rad/s while at a reference speed of 70 rad/s. Additional tuning of the controller would be necessary in order to see if the oscillations could be reduced further.

Acknowledgement
The authors of this work gratefully acknowledge Grundfos for sponsoring the 8^{th} MechMan symposium.

References

[1] Aalborg University 2021 AC Motor Drives course: Lecture 7 files: Appendix A: Mathematical Model.
[2] Electronics Tutorials: Kirchhoffs Voltage Law. URL: https://www.electronics-tutorials.ws/dccircuits/kirchhoffs-voltage-law.html.
[3] Lumen Learning: Magnetic Flux, Induction, and Faradays Law. URL: https://courses.lumenlearning.com/boundless-physics/chapter/magnetic-flux-induction-and-faradays-law.
[4] HØJRIS, A. G., STUPAKOWSKI, A., AND PENTEK, M. Design of Magnetic Gear with integrated Permanent Magnet Synchronous Machine for winch drive application. Master Thesis, 2020.
[5] KIM, S.-H. Electric Motor Control : DC, AC, and BLDC Motors. Elsevier, 2017.
[6] VOURNAS, D. G. Modeling and Control of Magnetic Gear Dynamics in a Wind Turbine Drivetrain.